Bulletin of the New Zealand Society for Earthquake Engineering, Vol. 55, No. 4, December 2022

EVALUATION OF A GEOSPATIAL LIQUEFACTION MODEL USING LAND DAMAGE DATA FROM THE 2016 KAIKŌURA EARTHQUAKE

Amelia Lin[1], Liam Wotherspoon[2] and Jason Motha[3]

(Submitted *June 2021*; Reviewed *August 2021*; Accepted *May 2022*)

ABSTRACT

The paper uses two geospatial liquefaction models based on (1) global and (2) New Zealand specific variables such as Vs30, precipitation and water table depth to estimate liquefaction probability and spatial extent for the 2016 Kaikōura earthquake. Results are compared to observational data, indicating that the model based on global variables underestimates liquefaction manifestation in the Blenheim area due to the low resolution of the input datasets. Furthermore, a tendency for underprediction is evident in both models for sites located in areas with rapidly changing elevation (mountainous terrain), which is likely caused by the low resolution of the elevation-dependent variables Vs30 and water table depth leading to incorrect estimates. The New Zealand specific model appears to be less sensitive to this effect as the variables provide a higher resolution and a better representation of region specific characteristics. However, the results suggest that the modification might lead to an overestimation of liquefaction manifestation along rivers (e. g. Kaikōura). An adjustment of the model coefficients and / or the integration of other resources such as geotechnical methods can be considered to improve the model performance. The evaluation of the geospatial liquefaction models demonstrates the importance of high-resolution input data and leads to the conclusion that the New Zealand specific model should be preferred over the original model due to better prediction performance. The findings provide an overall better understanding on the models' applicability and potential as a tool to predict liquefaction manifestation for future hazard assessments.

INTRODUCTION

Seismic events such as the 2008 Wenchuan earthquake [1], the 2011 Great East Japan earthquake [2,3], the 2012 Emilia earthquake [4,5] and the 2010–2011 Canterbury Earthquake Sequence [6,7] have demonstrated the impact of liquefaction and lateral spreading on the built environment. Damage can include the differential settlement of buildings and distortion of roads or buried infrastructure, emphasizing the need for an understanding of the potential extent and severity of liquefaction manifestation in order to support appropriate design decisions and emergency planning.

Liquefaction hazard maps are one of the main tools to represent liquefaction hazards across regions of interest. For the estimation of liquefaction triggering in specific soil layers and at a specific site, field investigation data and simplified methods are commonly used. Those methods can be based on standard penetration tests [8,9], cone penetration tests [10–12] or shear wave velocity [13,14]. For the wider assessment of liquefaction and the development of regional liquefaction hazard maps, geostatistical approaches and / or geological data can be incorporated [15–19]. However, as they require extensive resources, these methods might not be suitable for the analysis of large areas or networks [20].

Most recently, probabilistic models based on geospatial data are considered as an alternative approach. Zhu et al. [21] developed a geospatial liquefaction model by correlating case history data with globally accessible soil property data such as precipitation or water table depth. While the simplified liquefaction triggering methods calculate the probability or factor of safety of liquefaction in a specific layer within the soil profile, the geospatial model calculates the probability of surface manifestation. The representation of the presence of surface manifestation is more aligned to the outputs from the calculation of surface manifestation severity indices such as the Liquefaction Potential Index (LPI) and the Liquefaction Severity Number (LSN), amongst others [16,22,23]. The model was tested across different earthquake scenarios around the globe showing satisfying results, especially considering their time and cost related benefits over in-situ based approaches [22,24,25]. Differences in the interpretation of these outputs are discussed in more detail in the following section.

The evaluation of the geospatial model for different global events showed that the calculated estimates aligned with the liquefaction observations in many cases, demonstrating the model's potential as a time and cost efficient tool to predict the liquefaction probability [22,24,25]. Previous research assessed the model's prediction performance for the four major events of the 2010–2011 Canterbury Earthquake Sequence (CES) in Christchurch, New Zealand, and identified discrepancies regarding the quality of the global input variables. The use of region specific high-resolution datasets improved the spatial accuracy of the liquefaction hazard maps [26]. However, further validation is required to better understand the potential of the (modified) model.

This paper uses the geospatial model based on the global and New Zealand specific input variables to estimate liquefaction manifestation for the 2016 Kaikōura earthquake. The datasets

[1] *Corresponding author, PhD Candidate, University of Auckland, Auckland, alin116@aucklanduni.ac.nz. (Member)*
[2] *Associate Professor, University of Auckland, Auckland (Fellow)*
[3] *Software Engineer, University of Canterbury, Christchurch (Member)*

are presented and compared across the observation area. Prediction performance of each model is measured by comparing the calculated liquefaction probability and spatial extent with the observed liquefaction manifestation. The assessment is divided into two parts. First, the model performance is measured using a receiver operating classification (ROC) analysis for the Blenheim and Kaikōura area, where most of the liquefaction manifestation was observed (focus area). Second, to evaluate the models for the remaining cases, the entire observation area is assessed based on a neighbourhood analysis for the explanatory variables Vs30 and water table depth. The findings of both parts are compared to the performance results of the CES events by Lin et al. [26]. Limitations of the geospatial models regarding its applicability for national-scale liquefaction assessments are discussed, providing a better understanding of the model's potential as a tool to identify areas exposed to liquefaction in New Zealand.

GEOSPATIAL LIQUEFACTION MODEL

Using logistic regression analysis, Zhu et al. [21] correlated observational data from 27 earthquakes around the globe with geospatial data related to liquefaction manifestation. They found that the most promising results are achieved with a combination of peak ground velocity (PGV) in cm/s, shear wave velocity in the upper 30 m (Vs30) in m/s, annual precipitation (PRECIP) in mm, distance to the closest water body (DW) in km and water table depth (WTD) in m below ground level (m. b. g. l). The liquefaction probability (P) is calculated using the equation

$$\mathrm{P}(\mathrm{X}) = \frac{1}{1+e^{-}\mathrm{X}} \tag{1}$$

where X is a function of the explanatory variables

$$\begin{aligned}\mathrm{X} = {} & 8.801 + 0.334\,\ln(\mathrm{PGV}) - 1.918\,\ln(\mathrm{Vs30}) \\ & + 5.408\,10^{-4}\,\mathrm{PRECIP} - 0.2054\,\mathrm{DW} - 0.0333\,\mathrm{WTD}\end{aligned} \tag{2}$$

The liquefaction probability (P) describes the likelihood of surface manifestation. Assuming that liquefaction does not occur for very low ground shaking intensities or for very high Vs30, the model estimates a liquefaction probability of zero (P = 0) for PGV lower than 3 cm/s or Vs30 above 620 m/s. Further validation by Rashidian & Baise [25] showed that the model tends to overestimate liquefaction manifestation for large epicentral distances, high precipitation, and low magnitude events, which was addressed by introducing additional thresholds: liquefaction does not manifest for a peak ground acceleration lower than 0.1 g, PRECIP is restricted to a maximum value of 1 700 mm, and for events with a magnitude below 6, a magnitude scaling factor is applied for PGV.

In addition to the liquefaction probability, Zhu et al. [21] developed the liquefaction spatial extent (LSE) to describe the areal coverage (in percent) of surface manifestation. LSE is estimated by

$$\mathrm{LSE}(\mathrm{P}) = \frac{42.08}{(1+62.59\,e^{-11.43\,\mathrm{P}})^2} \tag{3}$$

where P is the liquefaction probability calculated by Equation 1. While the liquefaction probability allows for the assessment of past and future events on the basis of a binary classification analysis (liquefaction manifests versus liquefaction does not manifest), the liquefaction spatial extent can be used to illustrate the area that is potentially affected by liquefaction manifestation (percentage of raster cell covered by liquefaction manifestation), for example in order to develop liquefaction hazard maps for disaster risk management.

The geospatial model does not account for the liquefaction severity (e. g. minor to severe) or the liquefaction type (e. g. soil ejecta, cracking, etc.). Although it is likely that there is a link between these two characteristics and the LSE, the complexity of these processes exceeds the abilities of the geospatial approach.

The model was evaluated in detail for the major four events of the 2010–2011 Canterbury Earthquake sequence (CES) using ROC analysis and comparing the LSE maps with observational data [26]. Results suggest overall good performance for each earthquake scenario. However, the model is not able to directly represent the complexity of soil characteristics (e. g. interbedded layers with different liquefaction potential or seasonal changes in water table depth) as well as the effects of geomorphic features (e. g. constructed fills or historic channels) and seismic conditions (e. g. preceding earthquakes) [23,27], leading to potential discrepancies in the model outcome. Further limitations arise from the global input variables, which show a lack of spatial accuracy due to simplified methods and low resolution that are evident at a global scale. Lin et al. [26] proposed the use of New Zealand specific datasets for Vs30, DW and WTD to improve the model results for regional and local hazard assessments. Despite minor changes in the ROC performance, the increased spatial accuracy of the LSE maps supports the modification of the geospatial model.

DATA AND METHODOLOGY

Based on the geospatial model by Zhu et al. [21], liquefaction probability and spatial extent are calculated for the 2016 Kaikōura earthquake using both the global and the New Zealand specific variables. Prediction performance is evaluated by comparing the model results with observational data. Furthermore, the findings are discussed in relation to the assessment of the model performance for the CES events by Lin et al. [26]. The following sections focus on the processing of the observational data, the spatial differences between the global and the New Zealand specific input variables, and the data sampling as a requirement for the ROC analysis across the focus areas.

Observed Liquefaction Manifestation

The $\mathrm{M_W}$ 7.8 Kaikōura earthquake occurred on 14 November 2016, involving the rupture of multiple faults in the upper South Island of New Zealand. The rupture originated approximately 15 km north east of Culverden and propagated to the north-east along the east coast of Canterbury and Marlborough. The Kaikōura earthquake triggered tens of thousands of landslides [28] and caused wide ranging surface displacements, leading to severe damage of buildings and infrastructure networks [29–31]. Despite high shaking intensity, the extent of liquefaction and lateral spreading was relatively limited [32,33]. The QuakeCoRE historic liquefaction database [34] contains the observational data collected during post-event reconnaissance. The entries consist of different data formats including points (23 %), lines (e. g. roads, 60 %) and polygons (e. g. areas, 17 %), and describe both the land damage type (e. g. liquefaction without lateral spreading) and the liquefaction manifestation severity (e. g. minor). The database does not include the liquefaction manifestation and lateral spreading observed at CentrePort in Wellington [35].

Figure 1a presents an example of the data retrieved from the QuakeCoRE historic liquefaction database, showing an overlap

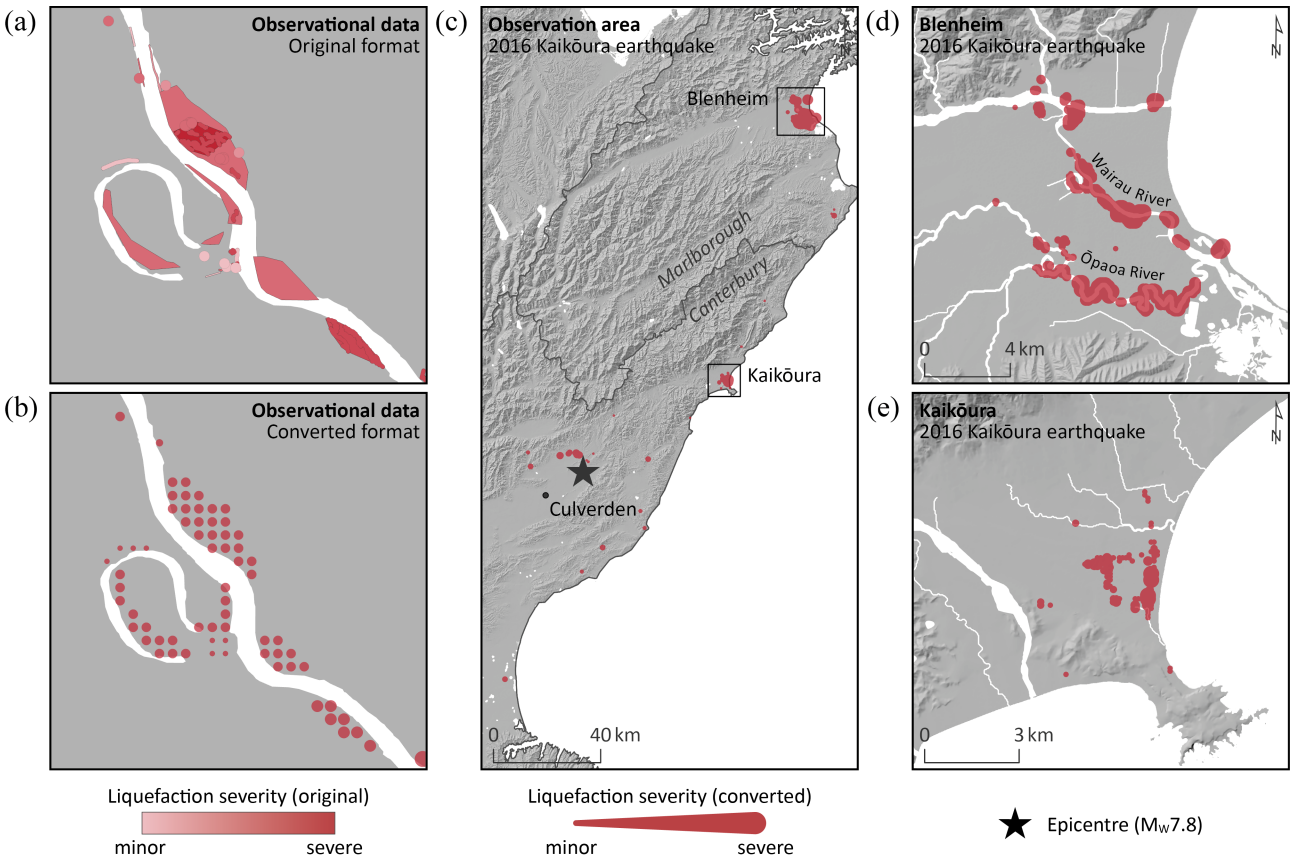

Figure 1: Illustration of the data processing from the (a) original format [34] to the (b) converted format, and observed liquefaction manifestation during the 2016 Kaikōura earthquake for the (c) observation area and the focus areas (d) Blenheim and (e) Kaikōura.

of different data formats (e. g. points and polygons). As the application of the geospatial liquefaction model requires a consistent data format, the lines and polygons are converted to points and point grids, respectively (Figure 1b, the point size indicates the severity of the observed liquefaction manifestation). The observational data that intersects water bodies is not considered in the converted data as some input datasets do not cover these areas. The point spacing along lines and the grid size across the polygons are set to 100 m in order to be in alignment with the resolution of the input variables. Overlapping datasets that could result in multiple points in one raster cell and potentially lead to information redundancy are treated as a single layer. All points are merged to one sample, leading to a final count of 416 points. The outcome of the conversion process for the observation area is shown in Figure 1c. Locations with observed liquefaction manifestation are scattered across the coastal region from the north of Marlborough to the north of the Canterbury region, as well as the area around the epicentre. Higher concentration of liquefaction manifestation (focus area) can be found in Blenheim (285 points) (Figure 1d) and Kaikōura (95 points) (Figure 1e). The observational data in Blenheim shows a higher manifestation severity, with most of the points located along the Wairau River (north) and the Ōpaoa River (south). The distribution pattern in Kaikōura does not directly relate to the surrounding rivers; however, many observation points are close to the eastern coastline.

Comparing the observational data of the 2016 Kaikōura earthquake with the liquefaction manifestation during the four CES events (4 September 2010, 22 February 2011, 13 June 2011 and 23 December 2011), three key differences can be identified. First, the observed liquefaction manifestation during the CES events is more extensive compared to the land damage of the Kaikōura earthquake. The CES dataset contains between 695 (4 September 2010) and 2 908 (22 February 2011) points where liquefaction manifested, leading to more reliable results for both the LSE and ROC analysis as they provide a better coverage of the area, hence, a better representation of the spatial features. The difference in sample size could lead to differences in the model performance when comparing the findings of 2016 Kaikōura earthquake with the CES events. Second, the CES data was collected on the basis of residential properties including sites with and without liquefaction manifestation. The Kaikōura data, on the other hand, only consists of positive cases (liquefaction manifested) and requires a sampling of negative cases (liquefaction did not manifest) to perform the ROC analysis (further details are discussed in the following section). Third, while the liquefaction manifestation during the CES events occurred on a relatively small area and close to the epicentre for each event, the land damage observed during the 2016 Kaikōura earthquake is much more geographically spread due to the number of faults involved and the geographic extent of the ruptures. Most of the liquefaction manifested in the Wairau Plains (Blenheim area), which mainly consists of alluvial soil similar to the Canterbury Plains; however, other sites with liquefaction manifestation are located across mountainous terrain, providing further insights into the model's prediction performance across different geological settings.

Explanatory Variables

The global datasets for PGV, which is estimated by the United States Geological Survey (USGS) ground motion and shaking intensity tool Shakemap [36], and PRECIP, which is retrieved from the global weather and climate database WorldClim [37], are used as both global (glo) and New Zealand specific (NZ)

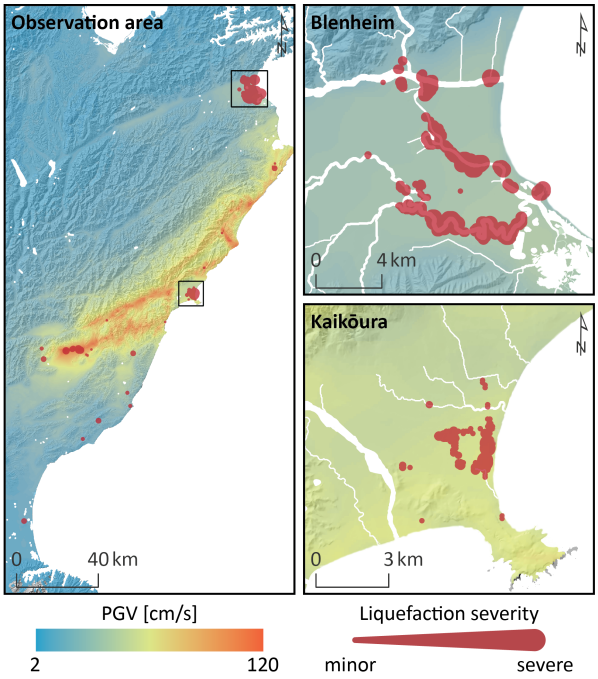

Figure 2: Peak ground velocity (PGV) during the 2016 Kaikōura earthquake.

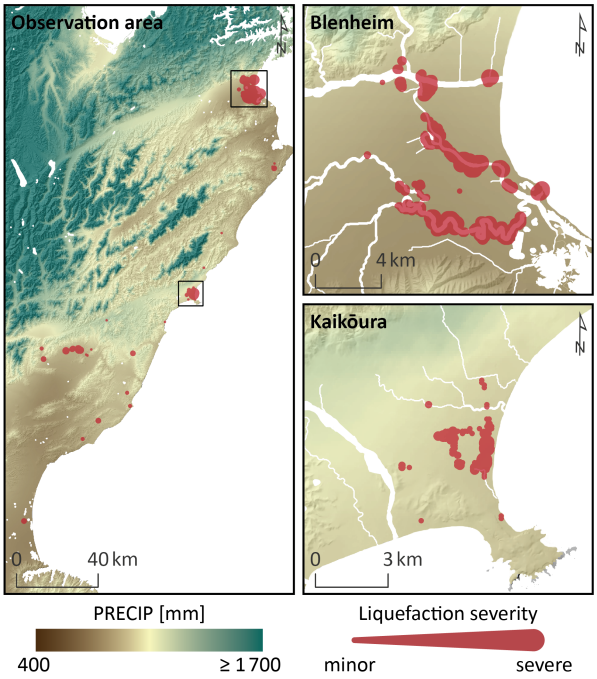

Figure 3: Precipitation (PRECIP).

input variables since no alternative sources are available for New Zealand.

While $Vs30_{glo}$ is based on the global approach by Wald & Allen [38], $Vs30_{NZ}$ is retrieved from the Vs30 map of New Zealand developed by Foster et al. [39]. The difference between the global and the region specific dataset is that $Vs30_{glo}$ uses a correlation with topographic slope, assuming that steeper gradients, which are more likely to occur in rock deposits, result in higher Vs30. $Vs30_{NZ}$ on the other hand, relies on both geology- and terrain-based variables and includes different sources of direct Vs30 measurements across New Zealand. It also offers a higher resolution (100 m) compared to $Vs30_{glo}$ (30 arcsec $\hat{=}$ 1 km).

WTD_{glo} is based on a groundwater model developed by Fan et al. [40], which uses climate, terrain and sea level to estimate water table depth on a global scale. Since the resolution of WTD_{glo} (30 arcsec $\hat{=}$ 1 km) might restrict its application for New Zealand, especially for areas with fast changing topography [41], Westerhoff et al. [42] developed a 200 m resolution water table map (WTD_{NZ}) that uses New Zealand specific input variables such as a national terrain model and long-term time series of recharge estimates.

DW is defined as the minimum of the distance to the closest river (DR) and the distance to the nearest coastline (DC). DR_{orig} is retrieved from the global platform Hydrological data and maps based on Shuttle Elevation Derivatives at multiple scales (HydroSHEDS) [43], which provides global hydrographic information. Apart from an inconsistent resolution (3 arcsec to 5 arcmin), the use of radar-based sources can lead to errors, for example in flat areas [44,45]. The calculation of DW_{NZ} is based on two national datasets: The New Zealand River Environment Classification provides the location of river lines, which were derived from a 30 m digital elevation model (DEM) and manually corrected by the National Institute of Water and Atmospheric Research (NIWA) [46]. As the resolution of this dataset is much higher compared to the global dataset that was used in the original liquefaction model, it is advised that only rivers of a stream order 4 or above should be used for the calculation of DR_{mod} to avoid overprediction [26]. The stream order represents the position of a river section in the entire network: 1 and 2 for headwater streams, 3 and 4 for tributaries, and 5 or greater for main stems [46]. The second dataset contains the water related areas (estuaries, lakes etc.) from the New Zealand Land Resource Information (LRNZ) [47], which better accounts for lakes and the areal extent of large rivers. The dataset to estimate DC is provided by Crown Minerals [48] and does not differ much from the global dataset [49] used by Zhu et al. [21]; however, its format (polylines) is more practical for the calculation of DC compared to the point format of the global dataset.

The datasets for the explanatory variables are converted to a raster and resampled using bilinear interpolation to achieve a consistent resolution of 100 m. While the Zhu et al. [21] approach uses a resolution of 30 arcsec, Rashidian & Baise [25] suggest that 3 arcsec (approx. 100 m) is more appropriate for the comparison with observational data, especially in fast changing terrains such as coastal areas. The maps of the explanatory variables for the observation and focus areas are shown in Figure 2 to 6. PGV (Figure 2) is very high (up to 120 cm/s) around the epicentre and along the eastern coastline following the direction of fault rupture. Despite showing higher liquefaction severity, the PGV values in Blenheim are lower than in Kaikōura. PRECIP (Figure 3) is low in all locations (PRECIP < 1250 mm), suggesting that the annual rainfall in the observation area does not significantly contribute to an increased liquefaction probability and spatial extent. $Vs30_{glo}$ (Figure 4a) is relatively low in both focus areas, especially in Blenheim (min $Vs30_{glo}$ = 180 m/s), which likely leads to a higher liquefaction susceptibility. $Vs30_{NZ}$ (Figure 4b) is even lower in this region with a minimum $Vs30_{NZ}$of 140 m/s. A wider range of values can be found for both $Vs30_{glo}$ and $Vs30_{NZ}$ in the locations with liquefaction manifestation outside the focus areas. WTD_{glo} (Figure 5a) and WTD_{NZ} (Figure 5b) are close to the ground level in both Blenheim and Kaikōura, with minimum values of 0 m. b. g. l., increasing the possibility of higher liquefaction estimates. Differences between the global and the New Zealand specific datasets are rather subtle across the two focus areas; however, WTD_{NZ} appears to be higher in

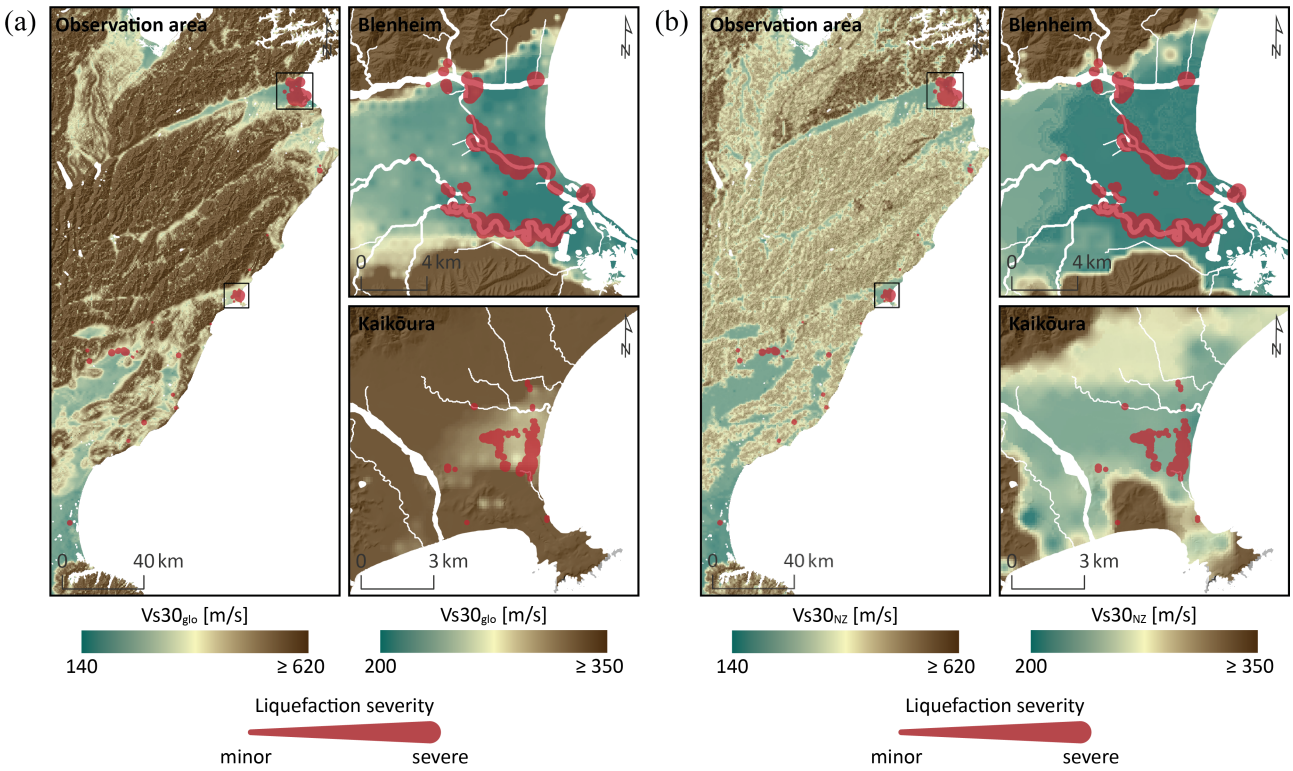

Figure 4: Vs30 based on the (a) global ($Vs30_{glo}$) and (b) New Zealand specific ($Vs30_{NZ}$) datasets. The scales are adjusted for the Blenheim and Kaikōura regions to better illustrate spatial differences.

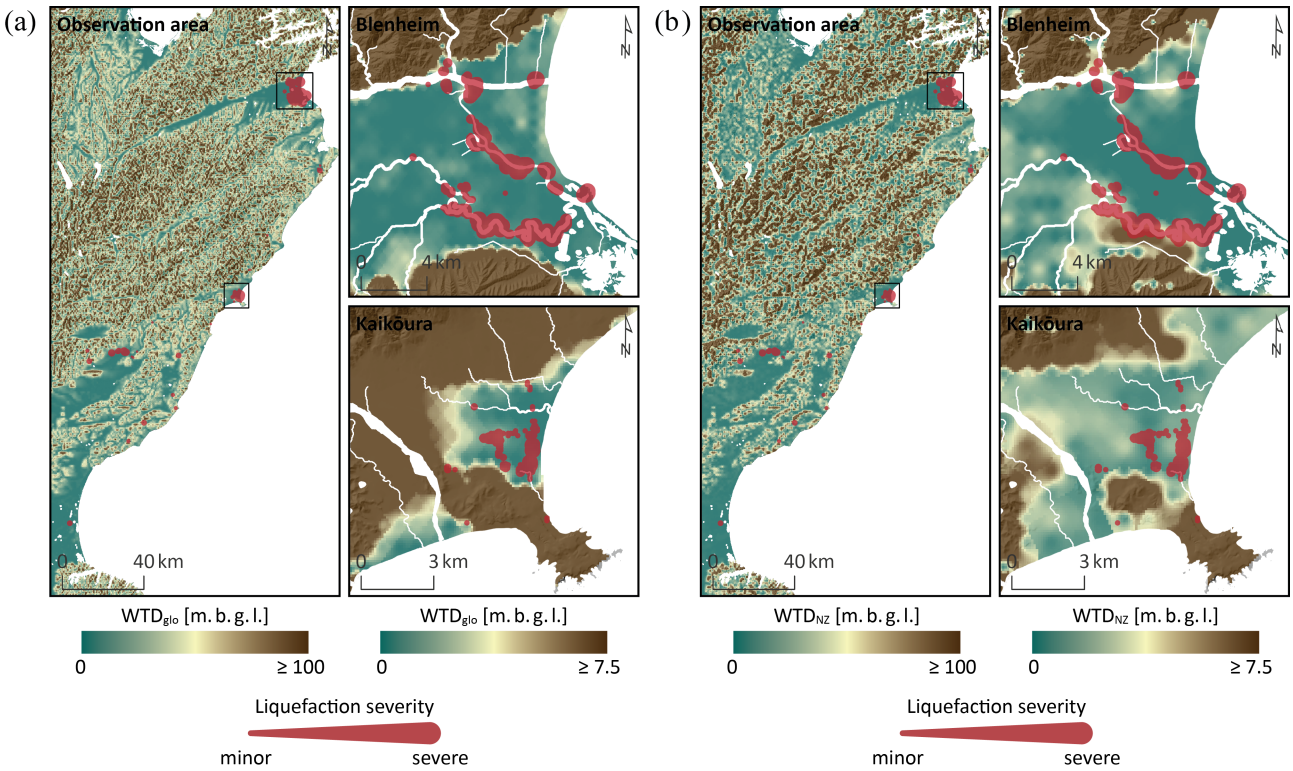

Figure 5: WTD based on the (a) global (WTD_{glo}) and (b) New Zealand specific (WTD_{NZ}) datasets. The scales are adjusted for the Blenheim and Kaikōura regions to better illustrate spatial differences.

the elevated regions, which could affect the model outcome for the locations outside the focus areas. DW across the observation area is primarily driven by DR. To better illustrate the impact of DR, the river datasets are presented as blue lines / polygons in the DW maps. DR_{glo} (Figure 6a) results in an oversimplification of the stream flow with the Wairau River (Blenheim) not being represented at all, leading to a higher DW_{glo} (up to 2.9 km) in this area. DR_{NZ} (Figure 6b), on the other hand, better represents the river flow and leads to lower DW_{NZ}, especially in Blenheim. Since most of the liquefaction manifestation was observed along

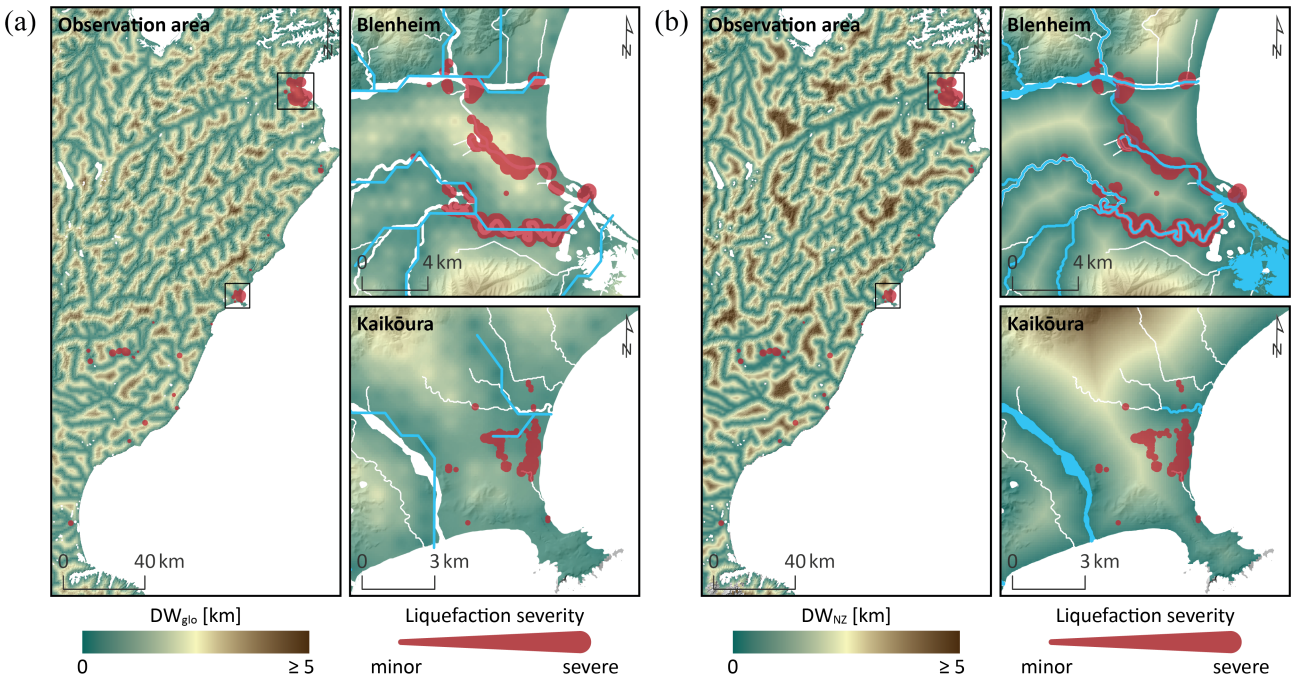

Figure 6: DW based on the (a) global (DW$_{glo}$) and (b) New Zealand specific (DW$_{NZ}$) datasets. The blue lines represent the river datasets used to calculate DR.

the rivers, it is assumed that the differences in the DR / DW datasets will significantly affect the model performance.

Sampled Data

The performance of the geospatial liquefaction models is assessed using a ROC analysis, a common tool to evaluate binary classification problems. Plotting the true positive rate (percentage of positives predicted correctly) against the false positive rate (percentage of negatives predicted incorrectly) for different probability thresholds results in the ROC curve. The area under the curve (AUC) indicates how well the models distinguish between positive (liquefaction manifested) and negative cases (liquefaction did not manifest). Usually, the ROC AUC ranges from 0.5 (random prediction) to 1.0 (perfect prediction). In addition to the AUC values, the optimal threshold (opt TH) is estimated and evaluated for each model. The optimal threshold is the probability value that best distinguishes between positive and negative cases. It can be used as a reference for the assessment of future earthquake scenarios. For instance, if a location results in an estimated liquefaction probability that is equal to or greater than the opt TH, liquefaction manifestation can be expected to occur. However, consistency in the optimal threshold for different areas and events is required to provide a robust reference. Both the ROC curve and the calculation of the opt TH are illustrated in Figure 7. Both the ROC AUC and the opt TH are compared to the ROC AUC / opt TH for all four CES events combined [26], referred to as the CES reference herein.

Since the observational data of the 2016 Kaikōura earthquake only consists of positive cases, additional points representing the negative sample are generated using spatial sampling. Zhu et al. [21] used random sampling, which involved the creation of buffers with a radius of 15 km around the positive cases. Across this area, random points were generated to represent the locations where no liquefaction manifested. A sensitivity analysis showed that the chosen radius did not affect the outcome of the ROC evaluation. However, due to the differences in spatial distribution of the observational data and the resolution of the explanatory

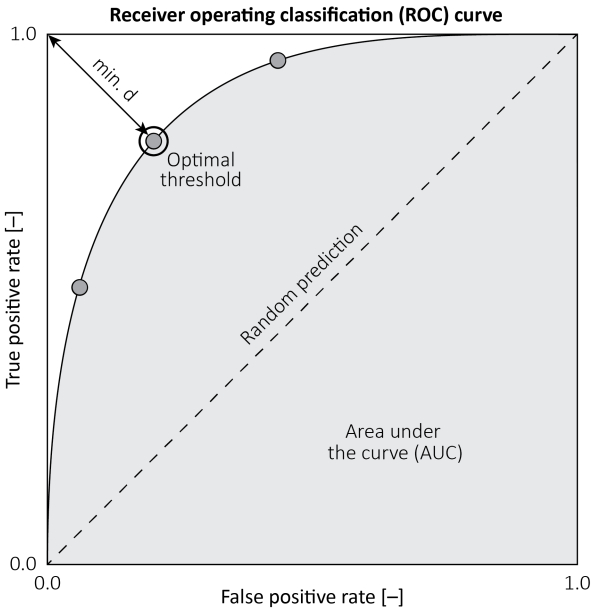

Figure 7: Illustration of the receiver operating classification (ROC) area under the curve (AUC) and the calculation of the optimal threshold (opt TH).

variables, the buffer dimensions proposed by Zhu et al. [21] are unsuitable for the assessment of the 2016 Kaikōura earthquake. Because of the higher point density in the focus areas, it is expected that the positive cases in these regions will result in similar probability values (positive spatial autocorrelation). A large buffer area would lead to a wider distribution of the negative cases, hence, a higher variation across the probability results and possibly a distortion of the ROC outcome. On the other hand, a small buffer area would not sufficiently cover the study area, limiting the validity of the assessment. To better account for these uncertainties, this paper uses the standard deviational ellipse, which summarizes spatial characteristics such as the

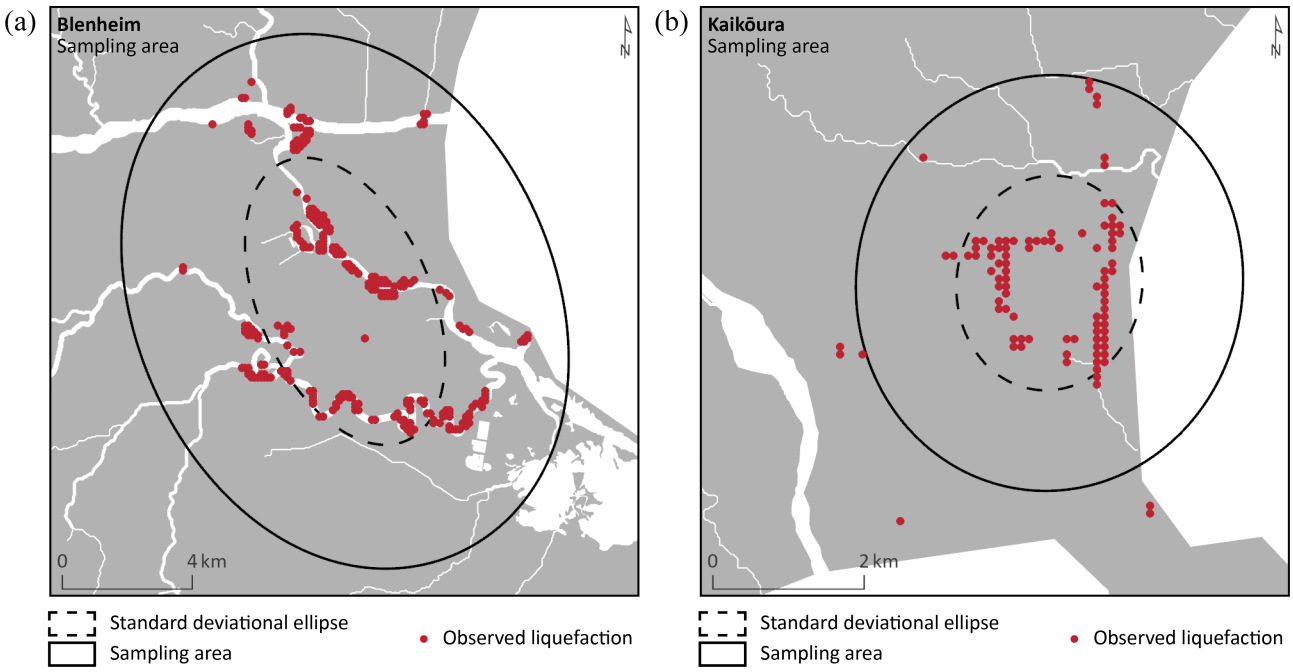

Figure 8: Illustration of the sampling method, including observed liquefaction manifestation for (a) Blenheim and (b) Kaikōura.

dispersion or directional trend of the positive cases, and the standard distance, which describes the compactness of the positive cases. The ellipse features are generated for the Blenheim and Kaikōura areas, and buffered to the standard distance for each sample in order to create the sampling areas (Figure 8). The data outside the focus areas is not suitable due to its small size (36 points) and large distribution, therefore, requires a different evaluation approach. A few positive cases in the Kaikōura region are outside the sampling area (Figure 8b), indicating that those might need to be considered spatial outliers. However, as the total area is relatively small, they remain in the sample. It is assumed that no liquefaction manifested in any location across the sampling areas (excl. water bodies) that is at least 100 m away from a positive case. The negative cases are generated by randomly selecting points from these locations. For class balance, the number of negative cases equals the number of positive cases. Although the ROC analysis is suitable for datasets with a skewed distribution, class balance is chosen to minimize the (spatial) bias towards the negative cases. To be in alignment with the (converted) observational data, an intersample distance of 100 m or above is chosen. Compared to the observational data of the CES events, which included both positive and negative cases, the assessment of the 2016 Kaikōura earthquake likely involves a higher level of uncertainty due to the sampling process, which needs to be considered when interpreting the ROC AUC results.

For both the positive and negative samples, the liquefaction probability is estimated in each point by extracting the values from the explanatory variable rasters and applying Equation 1 and 2. The ROC AUC is calculated to compare the model outcome of the global and New Zealand specific variables, and to further discuss the ROC performance for the 2016 Kaikōura earthquake with regard to the CES events.

RESULTS

Liquefaction probability and LSE are calculated for the 2016 Kaikōura earthquake using both the global and the New Zealand specific model. The LSE maps are compared to the observational data. Although LSE cannot be directly linked to the liquefaction severity, the comparison helps to discuss the models in a spatial context. For the Blenheim and Kaikōura area, a ROC analysis is used to evaluate the models' prediction potential based on the calculated liquefaction probability. For the remaining area, model performance is discussed using a more intuitive approach, involving of a more detailed evaluation of the explanatory variables Vs30 and WTD as well as a neighbourhood analysis.

Model Performance across Blenheim and Kaikōura

The ROC analysis is performed separately for the Blenheim and Kaikōura areas, since the AUC of a combined dataset would be biased towards the Blenheim samples due to their much larger size.

Original Explanatory Variables

Figure 9a presents the LSE maps for the observation area and the focus areas (Blenheim and Kaikōura) using the global explanatory variables. In Blenheim, higher values which imply that a larger area is affected by liquefaction manifestation can be found along the coast and the main river channels, for example the Ōpaoa River where many of the observation points are located. However, the low LSE around the remaining observation points (e. g. Wairau River) suggests a rather poor prediction performance. The underestimation is caused by the misleading river dataset, increasing DW_{glo} (Figure 6a) in the central part of Blenheim, which demonstrates the limitations of the global input variables and their use for regional or local liquefaction assessments. The LSE map of the Kaikōura area shows lower values, which aligns with the overall fewer observations of liquefaction manifestation across this region. However, in comparison to the range of LSE values covered in the Blenheim map (AUC $\leq$ 0.36), the LSE range of the Kaikōura map (AUC $\leq$ 0.15) is much shorter and might not properly reflect the observed extent of liquefaction manifestation.

The ROC curves of the original model are presented in Figure 9b. Both the Blenheim (0.64) and Kaikōura (0.71) samples lead to AUC below the CES reference (0.80), suggesting that the original model performs better for the 2010–2011 CES events than the 2016 Kaikōura earthquake. The relatively low AUC of

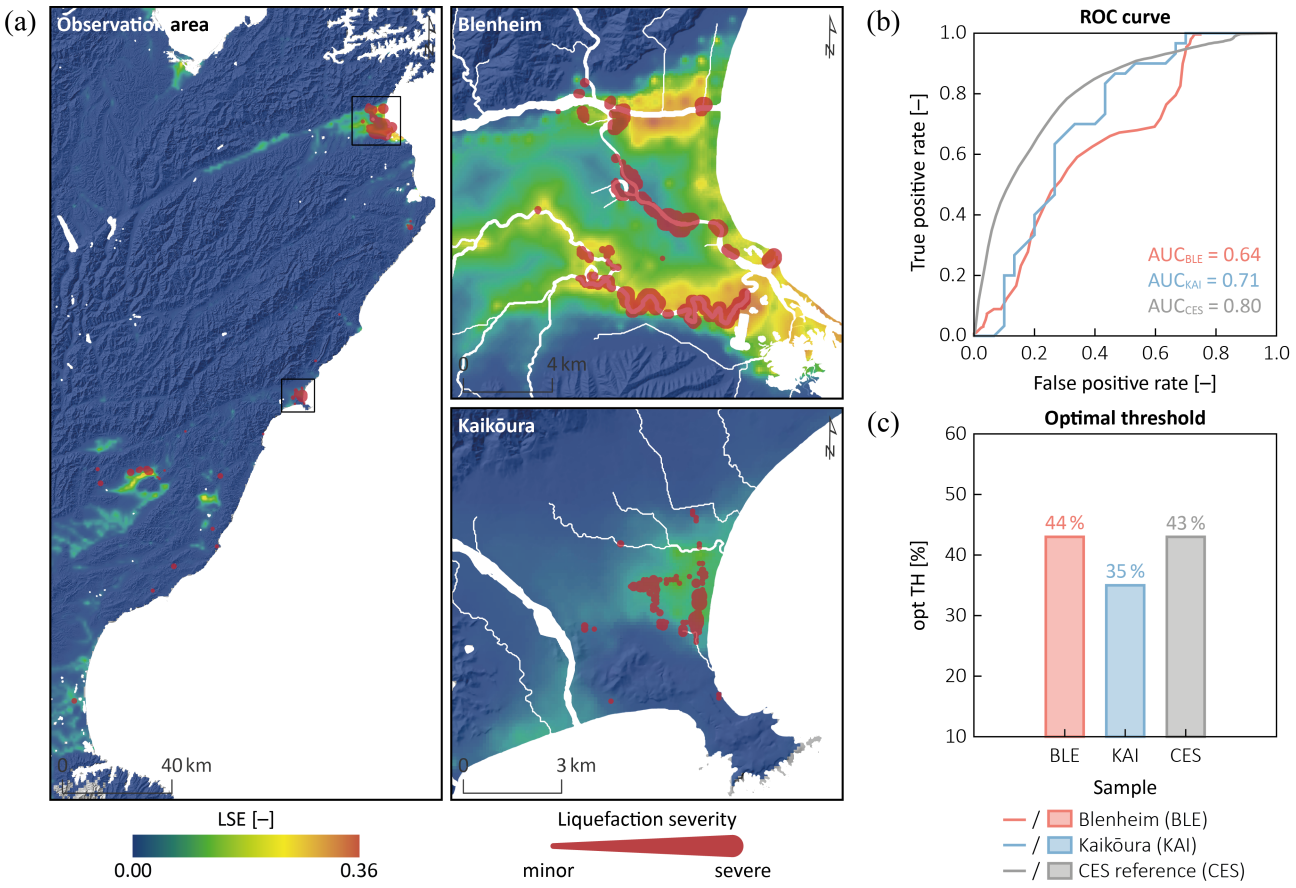

Figure 9: Results of the model performance analysis using the original model: (a) LSE including observed liquefaction manifestation, and (b) ROC curves and (c) opt TH for the Blenheim (BLE) and Kaikōura (KAI) area as well as the CES reference.

the Blenheim sample reflects the inconsistent results from the LSE map. The comparison of the optimal thresholds (Figure 9c) shows a similar value for the Blenheim region (44 %) and the CES reference (43 %), supporting the use of the opt TH for the assessment of future earthquakes. The opt TH of the Kaikōura region (35 %), on the other hand, is much lower as a result of the overall decreased liquefaction estimates. Applying the opt TH of the other samples would lead to an underestimation of the liquefaction hazard in this area, reducing the prediction performance of the original model.

Modified Explanatory Variables

Figure 10a presents the LSE map of the observation area using the modified model, showing higher values in the north, in scattered areas along the east coast, and around the epicentre. The outcome is similar to the LSE map in Figure 9a; however, values in the modified LSE map are overall higher. The LSE distribution in Blenheim aligns well with the observational data, showing hotspot areas along the Wairau River and Ōpaoa River. However, higher LSE is also presented in regions where no liquefaction manifested, for example, north east of the Wairau River or along the coast. The LSE map of Kaikōura shows higher values despite the lower ground shaking intensity and the fewer cases of liquefaction manifestation observed in this area. The increased LSE along the east coast aligns well with the observational data. However, high values can also be found along the coast in the north and along the water stream in the east, where no liquefaction manifested, indicating that the model might overestimate liquefaction manifestation. It is likely that the low $Vs30_{NZ}$ (Figure 4b) and DW_{NZ} (Figure 6b) are the reason for the high LSE in these areas.

The ROC curves of the modified model (Figure 10b) show a significantly higher AUC for the Blenheim sample (0.75) compared to the original model, which is the result of the better representation of the liquefaction manifestation along the Wairau River. Despite the evident differences in the LSE maps, the modified model leads to the same ROC AUC for the Kaikōura sample (0.71), indicating similar prediction potential. However, the ROC analysis does not cover the eastern area where LSE map demonstrates an overprediction of liquefaction manifestation along the river (Figure 10a). Again, the values cannot reach the AUC of the CES reference (0.82). Following the overall increased liquefaction estimates, the opt TH for all samples are higher (Figure 10c) with values of 48 % and 46 % for the Blenheim and Kaikōura areas, respectively. In contrast to the opt TH of the original model, they provide more consistency when compared to the CES reference (50 %), leading to the conclusion that the modified model likely results in a better prediction performance for the Kaikōura region.

The comparison of the LSE maps and the ROC analysis suggest that the modified model performs better than the original model as it better represents the observed liquefaction manifestation and provides higher AUC values as well as more certainty in the opt TH. However, the ROC results emphasize that the prediction performance for the 2016 Kaikōura earthquake is not as high as the 2010–2011 CES events. Furthermore, the tendency for overestimation shows potential for improvement, especially for areas close to water bodies where the model does not effectively distinguish between positive and negative cases. Other data sources could be integrated to better account for geotechnical details in the soil profile and to reduce the risk of false prediction. For example, Rashidian and Baise [25] found that a liquefaction

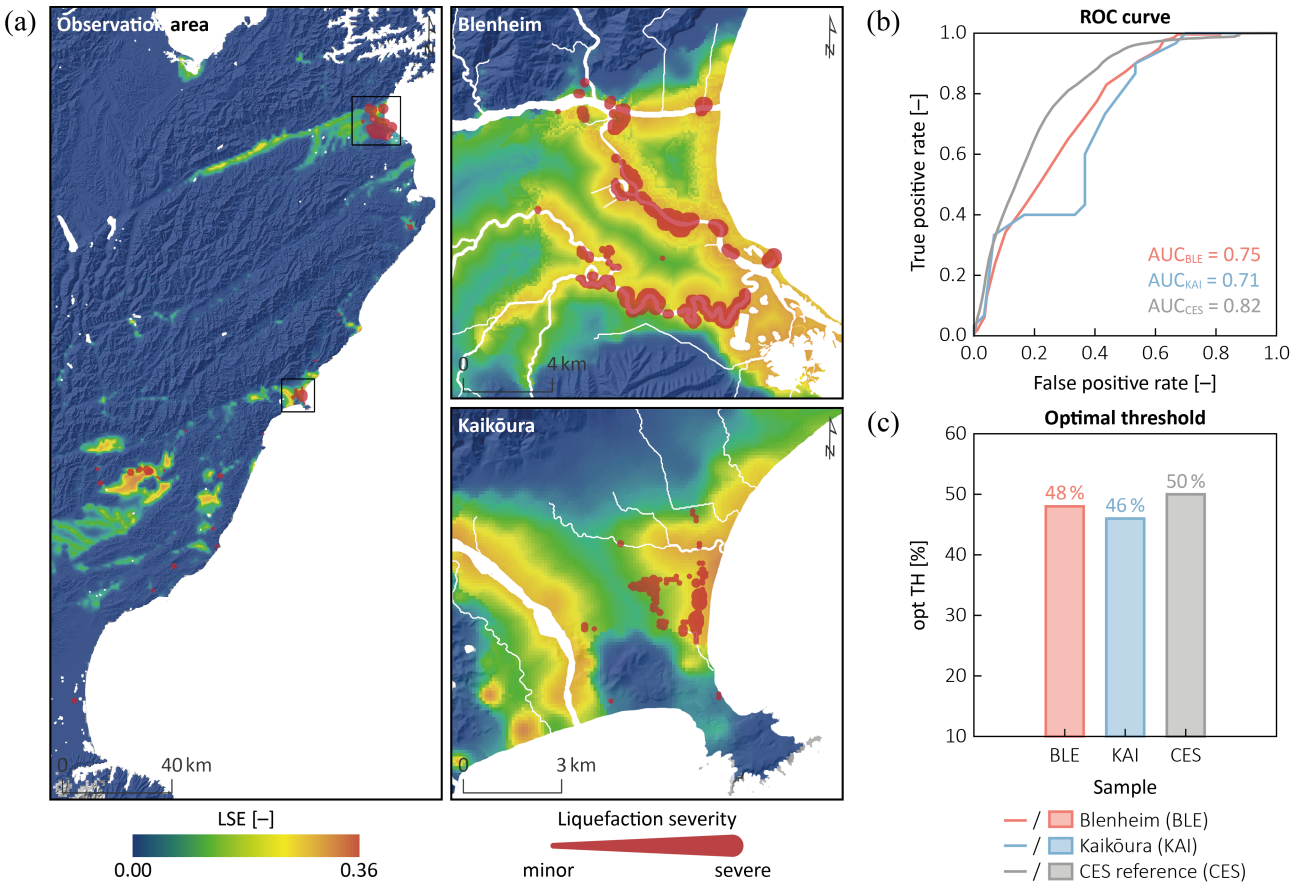

Figure 10: Results of the model performance analysis using the modified model: (a) LSE including observed liquefaction manifestation, and (b) ROC curves and (c) opt TH for the Blenheim (BLE) and Kaikōura (KAI) area as well as the CES reference.

potential index (LPI) map based on cone penetration testing based triggering analysis better reflects the heterogeneity of the soil across the Christchurch region.

Model Performance across the Entire Observation Area

Outside Blenheim and Kaikōura, the LSE map of both models show increased values for the positive cases close to the epicentre. However, the locations of positive cases scattered along the coast have very low LSE values, indicating inconsistencies in the model's prediction performance. Considering that these cases are surrounded by mountainous terrain in areas with variable topography, the underestimation of liquefaction may be caused by the false estimates of the topography dependent variables Vs30 and WTD. This section focuses on the variation of Vs30 and WTD in the positive samples, and analyses the change in elevation in the neighbourhood (surrounding area) of the positive cases.

Distribution of Vs30 and WTD

While Vs30 is expected to be higher in elevated areas due to the presence of rock, WTD naturally increases with elevation moving away from water bodies. Figure 11 shows the distribution of Vs30 and WTD as box plots (excl. outliers) for the positive samples of the Blenheim (BLE) and Kaikōura (KAI) areas as well as the remaining cases outside these areas (OUT). To compare the explanatory variables in a wider context, the plots also include a CES sample, a subset of the CES reference that contains the locations that liquefied during at least one of the CES events [26]. While the maps in Figure 4 and 5 illustrate the spatial distribution of each variable, the box plots provide a better visualisation of the quantitative differences across the samples.

For Vs30 (Figure 11a), the original dataset leads to a similar median for the BLE sample (median $Vs30_{glo}$ = 212 m/s) and the CES sample (median $Vs30_{glo}$ = 222 m/s). The KAI sample shows a slightly higher value (median $Vs30_{glo}$ = 311 m/s), which could explain the overall lower liquefaction probability and LSE in this area. All three plots have a similar range (values between the minimum and the maximum value). The plot of the OUT sample results in both a higher median $Vs30_{glo}$ of 375 m/s and a wider range with values up to $Vs30_{glo}$ = 695 m/s, which could be explained by the low resolution of the input dataset not properly capturing the fast changing topography, hence, smearing $Vs30_{glo}$ in this area. This effect is likely amplified by the fact that $Vs30_{glo}$ is derived from slope. For the modified dataset, the CES sample shows the overall lowest median with $Vs30_{NZ}$ = 189 m/s. The BLE and KAI samples lead to slightly lower values compared to the global (median $Vs30_{NZ}$ = 203 m/s and $Vs30_{NZ}$ = 232 m/s, respectively). Also, the range is smaller as values remain constant across Blenheim and Kaikōura. Similar to $Vs30_{glo}$, $Vs30_{NZ}$ shows a wider range of values for the OUT sample; however, the variation is not as significant, which could be the result of a higher resolution and / or due to the assumption that the modified model is less biased towards slope. Moreover, the median is much closer to the other samples.

Compared to Vs30, WTD has a minor contribution to the calculation of the liquefaction probability and LSE. However, it increases quickly with elevation. As presented in Figure 11b, the box plots of the OUT sample show a wider range in WTD_{glo} and WTD_{NZ}. In contrast to $Vs30_{glo}$ and $Vs30_{NZ}$, both the range and

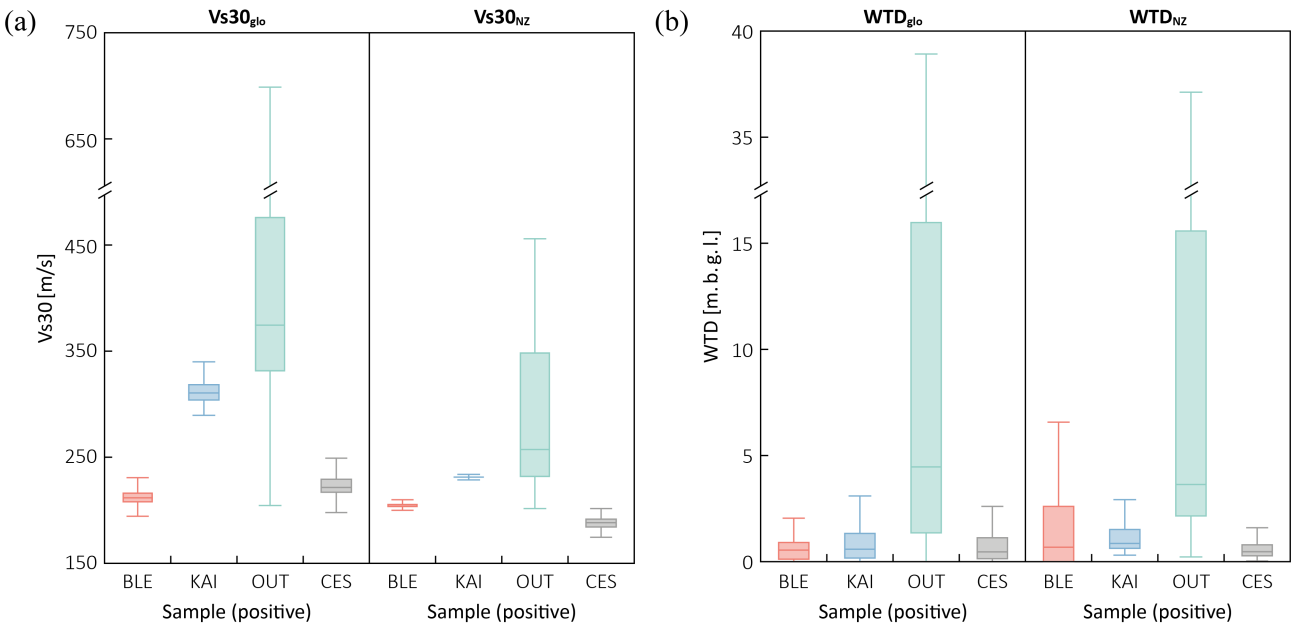

Figure 11: Distribution of (a) Vs30 and (b) WTD for the positive samples of the 2016 Kaikōura earthquake based on the global and New Zealand specific explanatory variables.

the median of the original and the modified WTD are similar. In addition, the positive skewness is more distinct, indicating that the higher values (above the median) are more dispersed, which supports the assumption that WTD_{glo} / WTD_{NZ} increase abruptly as a result of a fast changing terrain and elevation. For the BLE, KAI and CES samples, the median of WTD_{glo} and WTD_{NZ} are below 1 m. b. g. l. The BLE sample based on the New Zealand specific variable leads to a slightly wider range with a maximum WTD_{NZ} of approx. 7 m. b. g. l. This is likely caused by the slightly elevated areas in the north and south of the Blenheim area.

The wider range and the positive skewness of the positive cases outside the Blenheim and Kaikōura areas (OUT) suggest that Vs30 and WTD are affected by the fast changing elevation in the mountainous areas. It is possible that the resolution of the input variables is not able to properly capture the Vs30 and WTD of lower areas that are surrounded by mountains (e. g. river valleys), leading to increased Vs30 and WTD values, hence, decreased liquefaction probability and LSE for locations where liquefaction manifestation was observed.

Neighbourhood Analysis

In order to better understand the influence of a fast changing environment on Vs30, WTD and, ultimately, on the model outcome, the neighbourhood of each positive case is analysed with respect to its variation in elevation. Based on the digital elevation model (DEM) by Land Information New Zealand [50], a 100 m resolution elevation raster is created across the observation area. For each cell, the standard deviation of the elevation (SD_{DEM}) of the surrounding cells in a 1 000 m radius is calculated. SD_{DEM} indicates how fast the neighbourhood of a particular location changes. Flat areas result in lower SD_{DEM}, mountainous areas in higher SD_{DEM}. Figure 12 presents the variation of SD_{DEM} with respect to the calculated liquefaction probability (P) for the positive cases of the BLE, KAI and OUT samples. The BLE sample shows the lowest values with an average SD_{DEM} of 2 m, while the KAI sample leads to slightly higher results (average SD_{DEM} = 5 m). Both samples confirm a relatively stable elevation across the Blenheim and Kaikōura areas. The OUT sample, on the other hand, presents a wider range of SD_{DEM} from 1 m to 109 m. For the original model (Figure 12a), a few cases of the KAI sample with a lower liquefaction probability (P < opt TH) have increased SD_{DEM} values (SD_{DEM} > 10 m). The same trend can be observed for the OUT sample, which supports the assumption that cases in areas with fast changing elevation tend to result in lower probabilities regardless of whether liquefaction manifested or not. A similar conclusion can be drawn for the modified model (Figure 12b). However, the cases of all samples are shifted to the right (higher liquefaction probability), indicating that the effect of SD_{DEM} is less significant compared to the original model. Primarily, positive cases with a SD_{DEM} of 20 m or above show a clear tendency to result in lower liquefaction probability.

To visualize SD_{DEM} in a spatial context, Figure 13 presents SD_{DEM} across the observation area including the estimated liquefaction probability (P) of the positive cases. The magenta area has a SD_{DEM} of 10 m or above for the original model (Figure 13a) and a SD_{DEM} of 20 m or above for the modified model (Figure 13b). The observation sites with the lowest liquefaction probability ($P \leq 0.2$) are scattered across this area, while points with higher liquefaction probability (P > 0.3) are located in regions with lower SD_{DEM} such as Blenheim, Kaikōura and the area around the epicentre. Considering SD_{DEM} as a potential threshold to identify regions that could lead to false liquefaction estimates, the affected area covers most of the South Island, which is dominated by mountains. Although liquefaction manifestation is less likely to occur in this region, the findings of the SD_{DEM} assessment show that the models might not produce reliable results for large areas in New Zealand.

The Canterbury Plains show overall low SD_{DEM} values. For most of the locations with liquefaction manifestation during the CES, the SD_{DEM} is below 10 m. As it is unclear how higher SD_{DEM} could affect the model outcome of these events, a cross validation is not possible.

DISCUSSION

The geospatial liquefaction model by Zhu et al. [21] was used to calculate liquefaction probability and LSE for the 2016 Kai-

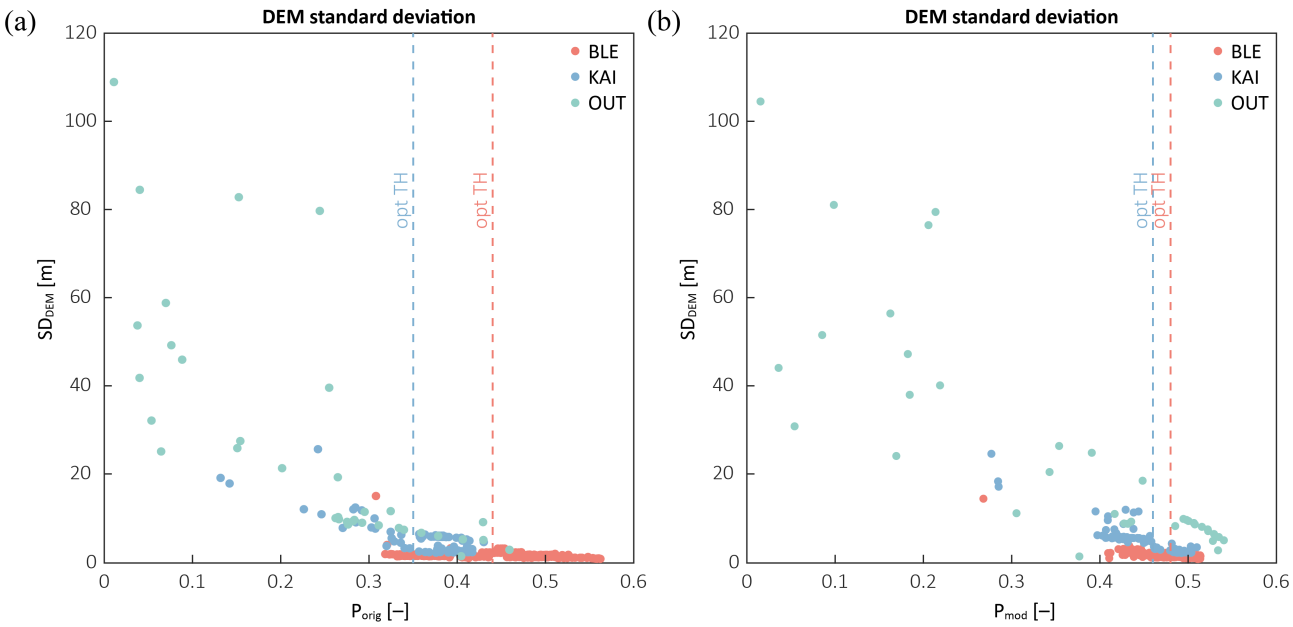

Figure 12: DEM standard deviation (SD_{DEM}) over the liquefaction probability (P) for the positive cases of the 2016 Kaikōura earthquake using the (a) original and (b) modified models, including the opt TH for the Blenheim and Kaikōura samples.

kōura earthquake based on the global and New Zealand specific explanatory variables. Comparing the LSE maps with observational data across Blenheim and Kaikōura shows discrepancies related to the low spatial accuracy of DW_{glo}, highlighting the importance of high quality input datasets. The LSE maps of the modified model better capture regions where liquefaction manifestation was observed. However, it tends to overpredict in areas close to water bodies.

Although the soil conditions in the Blenheim and Kaikōura areas are similar to the Canterbury Plains, the ROC results indicate that the original and modified models perform better for the CES events. The comparison demonstrates that that the model performance in one location is not necessarily representative for another location. However, it should be noted that the ROC results of the 2016 Kaikōura earthquake hold a higher level of uncertainty due to the much smaller sample size and the lack of directly observed negative cases. Furthermore, the ROC AUC results are likely biased due to the sampling approach, especially for the Kaikōura sample which is very small in terms of number of cases and the area covered by the assessment. Therefore, it is important to evaluate the prediction performance based on both the ROC AUC / opt TH and the LSE maps. For example, although the original and the modified model lead to relatively high AUC values (0.71) for the Kaikōura region, the results overestimate the prediction performance as illustrated by the inconsistent opt TH in the original model and by the overprediction in the LSE map of the modified model. In addition, the assumption that the observational data was comprehensive, implying that no liquefaction manifestation occurred in any location outside the observation area, increases the uncertainty of the performance results as well. Despite the limitations, particularly for the Kaikōura sample, the findings demonstrate the benefits of region specific input variables over the global datasets and the model's potential for further improvements.

In order to better understand its applicability on a national level, the model needs to be further evaluated for more earthquake case histories. This should also include investigating potential impacts of using New Zealand specific input datasets over the global variables. Since the model was trained on the global datasets, an adjustment of the coefficients in Equation 2 might be appropriate to better account for the changes in liquefaction probability and spatial extent caused by the modified model. For example, DW_{NZ} appears to significantly increase LSE along water bodies (e. g. Kaikōura) and might lead to overprediction of liquefaction manifestation. Using case histories across New Zealand (e. g. the QuakeCoRE historic liquefaction database), the model could be adjusted by performing a regression analysis based on the New Zealand specific datasets. This could also provide more details on the correlation behaviour of each variable, helping to better understand their prediction potential.

Moreover, the potential link between P / LSE and the observed liquefaction severity could be further investigated and might improve the model as a tool to generate hazard maps. As the severity depends on subsurface factors such as the depth and thickness of liquefiable layers or the presence of both liquefiable and non-liquefiable layers, other metrics (e. g. LPI) may need to be incorporated to represent soil profile characteristics. However, current methods based on site specific geotechnical data are also restricted in their ability to accurately predict liquefaction manifestation [51]; thus, cannot fully compensate for the limitations of the geospatial model.

The neighbourhood analysis of the observed liquefaction manifestation during the 2016 Kaikōura earthquake outside the focus areas shows decreased liquefaction estimates in mountainous terrain (SD_{DEM} > 10 m for the original model and SD_{DEM} > 20 m for the modified model), leading to the conclusion that WTD and Vs30 are not able to capture the areas where the change in topography is more rapid than the grid spacing of the input variables. Although liquefaction manifestation is expected to be less likely, the smearing of properties can influence the prediction results. However, more observational data for different terrain is required to better understand the impact of rapidly changing topography on the model performance. For example, based on the assessment of 2016 Kaikōura earthquake, the "threshold" to determine which areas are more likely to underestimate liquefaction probability and LSE is SD_{DEM} = 10 m and 20 m for the original and the modified model, respectively. This thresh-

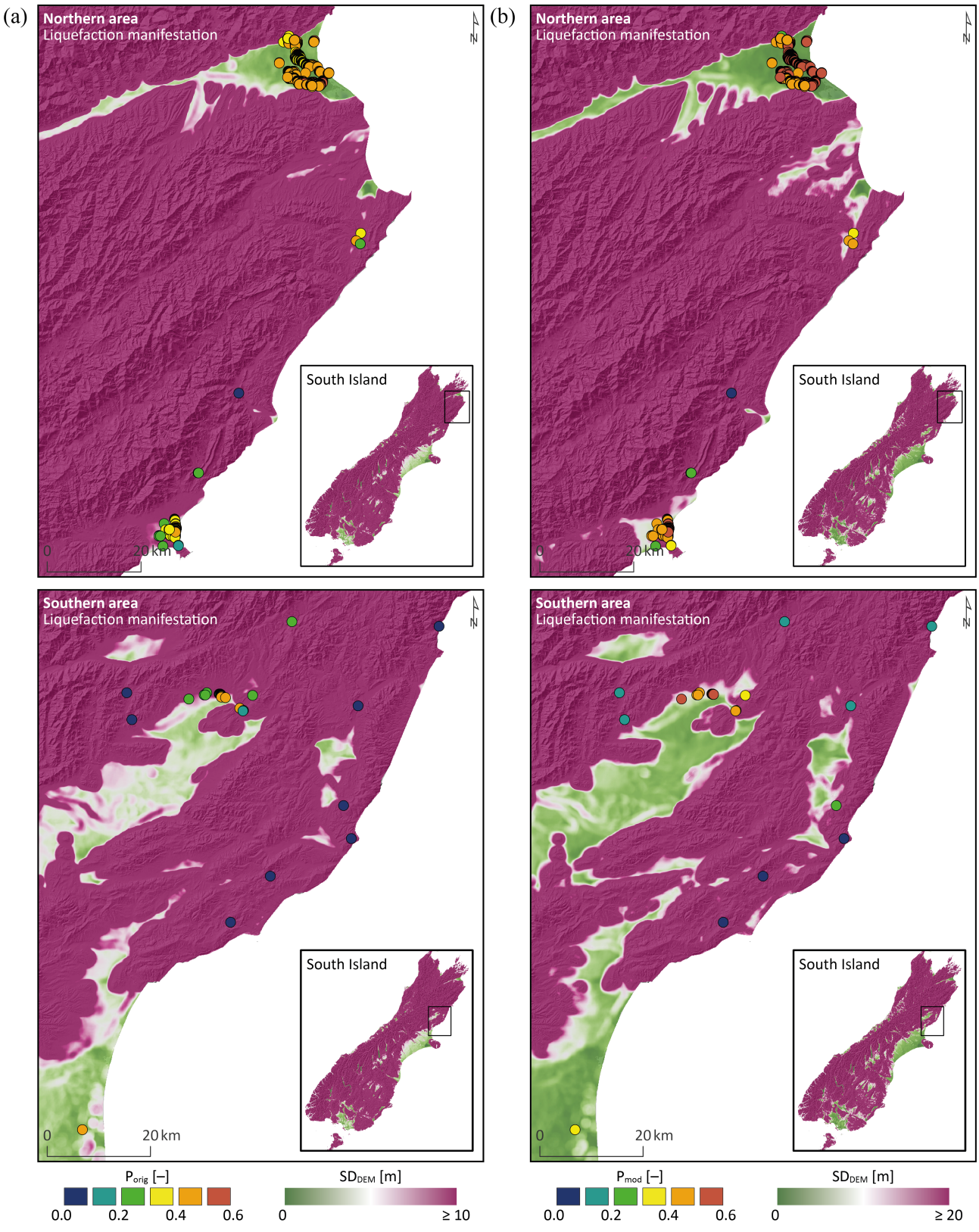

Figure 13: DEM standard deviation (SD_{DEM}) and liquefaction probability (P) of the observed liquefaction manifestation during the 2016 Kaikōura earthquake for the (a) original and (b) modified models.

old might vary for other earthquakes scenarios, changing the interpretation of the model results.

The findings help to better understand the (modified) geospatial liquefaction model by Zhu et al. [21] regarding its applicability for New Zealand, highlighting limitations such as the uncertainties across mountainous terrain and emphasizing the potential for further improvement, for example, by incorporating more data that represents soil profile characteristics in order to further refine the model's development. Although the modified model allows for a rapid estimation of liquefaction hazards, which can be used for large-scale assessments, the limitations demonstrate that the model is not suitable as a stand-alone tool for site-specific

assessments. In these cases, geotechnical investigation data and the current state-of-practice liquefaction evaluation procedures should be utilised.

CONCLUSION

The evaluation of the 2016 Kaikōura earthquake provides a better understanding of the geospatial liquefaction models and their applicability across different areas in New Zealand. Based on the ROC analysis and neighbourhood assessment, the modified model is preferred over the original model because of the high-resolution and / or more updated input variables, which lead to higher AUC values, a more consistent opt TH and a lower sensitivity to smearing Vs30 and WTD across fast changing topography. However, the tendency for overprediction along water bodies and the potential underestimation across mountainous terrain highlight the uncertainty in the calculated liquefaction probability and LSE and the need for further research. Although more observational data is required to validate the results and assess the prediction performance across other areas in New Zealand, the findings support the use of region specific datasets in order to improve the model outcome. The modified model allows for a time- and cost-efficient estimation of liquefaction hazards for regional and national assessments. However, due to the uncertainties, it should be mainly applied as a high-level screening tool or in combination with other resources.

ACKNOWLEDGMENTS

This project was supported by the University of Auckland Doctoral Scholarship and by QuakeCoRE, a New Zealand Tertiary Education Commission-funded Centre. This is QuakeCoRE publication number 0673. The work greatly benefited from the data provided by Sjoerd Van Ballegooy.

REFERENCES

1 Chen L, Yuan X, Cao Z, Hou L, Sun R, Dong L, Wang W, Meng F and Chen H (2009). "Liquefaction macrophenomena in the great Wenchuan earthquake". *Earthquake Engineering and Engineering Vibration*, **8**(2): 219–229. https://doi.org/10.1007/s11803-009-9033-4

2 Boulanger R (2012). "Liquefaction in the 2011 Great East Japan earthquake: Lessons for U.S. practice". *International Symposium on Engineering Lessons Learned from the 2011 Great East Japan Earthquake (2012, March 1–4)*, Tokyo, Japan. https://www.jaee.gr.jp/event/seminar2012/eqsympo/pdf/papers/187.pdf

3 Yasuda S, Harada K, Ishikawa K and Kanemaru Y (2012). "Characteristics of liquefaction in Tokyo Bay area by the 2011 Great East Japan Earthquake". *Soils and Foundations*, **52**(5): 793–810. https://doi.org/10.1016/j.sandf.2012.11.004

4 Di Ludovico M, Chiaradonna A, Bilotta E, Flora A and Prota A (2020). "Empirical damage and liquefaction fragility curves from 2012 Emilia earthquake data". *Earthquake Spectra*, **36**(2): 507–536. https://doi.org/10.1177\%2F8755293019891713

5 Fontana D, Amoroso S, Minarelli L and Stefani M (2019). "Sand liquefaction induced by a blast test: New insights on source layer and grain-size segregation mechanisms (late quaternary, Emilia, Italy)". *Journal of Sedimentary Research*, **89**(1): 13–27. https://doi.org/doi.org/10.2110/jsr.2019.1

6 Cubrinovski M, Robinson K, Taylor M, Hughes M and Orense R (2012). "Lateral spreading and its impacts in urban areas in the 2010–2011 Christchurch earthquakes". *New Zealand Journal of Geology and Geophysics*, **55**(3): 255–269. https://doi.org/10.1080/00288306.2012.699895

7 Orense RP, Kiyota T, Yamada S, Cubrinovski M, Hosono Y, Okamura M and Yasuda S (2011). "Comparison of liquefaction features observed during the 2010 and 2011 Canterbury earthquakes". *Seismological Research Letters*, **82**(6): 905–918. https://doi.org/10.1785/gssrl.82.6.905

8 Cetin KO, Seed RB, Der Kiureghian A, Tokimatsu K, Harder LF, Kayen RE and Moss RES (2004). "Standard penetration test-based probabilistic and deterministic assessment of seismic soil liquefaction potential". *Journal of Geotechnical and Geoenvironmental Engineering*, **130**(12): 1314–1340. https://doi.org/10.1061/(ASCE)1090-0241(2004)130:12(1314)

9 Idriss I and Boulanger R (2008). *Soil Liquefaction during Earthquakes*. Earthquake Engineering Research Institute (EERI), Oakland, CA.

10 Boulanger R and Idriss IM (2014). *CPT and SPT based liquefaction triggering procedures*. Report Report No. UCD/CGM.-14/01, Center for Geotechnical Modelling, Civil & Environmental Engineering, UC Davis, CA. http://www.ce.memphis.edu/7137/PDFs/Notes/i3Boulanger_Idriss_CPT_and_SPT_Liq_triggering_CGM-14-01_20141.pdf

11 Moss RE, Seed RB, Kayen RE, Stewart JP, Der Kiureghian A and Cetin KO (2006). "CPT-based probabilistic and deterministic assessment of in situ seismic soil liquefaction potential". *Journal of Geotechnical and Geoenvironmental Engineering*, **132**(8): 1032–1051. https://doi.org/10.1061/(ASCE)1090-0241(2006)132:8(1032)

12 Robertson PK and Wride CE (1998). "Evaluating cyclic liquefaction potential using the cone penetration test". *Canadian Geotechnical Journal*, **35**(3): 442–459. https://doi.org/10.1139/t98-017

13 Andrus RD and Stokoe II KH (2000). "Liquefaction resistance of soils from shear-wave velocity". *Journal of Geotechnical and Geoenvironmental Engineering*, **126**(11): 1015–1025. https://doi.org/10.1061/(ASCE)1090-0241(2000)126:11(1015)

14 Kayen R, Moss RES, Thompson EM, Seed RB, Cetin KO, Der Kiureghian A, Tanaka Y and Tokimatsu K (2013). "Shear-wave velocity-based probabilistic and deterministic assessment of seismic soil liquefaction potential". *Journal of Geotechnical and Geoenvironmental Engineering*, **139**(3): 407–419. https://doi.org/10.1061/(ASCE)GT.1943-5606.0000743

15 Bastin SH, van Ballegooy S, Mellsop N and Wotherspoon L (2020). "Liquefaction case histories from the 1987 Edgecumbe earthquake, New Zealand – Insights from an extensive CPT dataset and paleo-liquefaction trenching". *Engineering Geology*, **271**(2020): 105404. https://doi.org/10.1016/j.enggeo.2019.105404

16 Holzer TL, Bennett MJ, Noce TE, Padovani AC and Tinsley Iii JC (2006). "Liquefaction hazard mapping with LPI in the Greater Oakland, California, area". *Earthquake Spectra*, **22**(3): 693–708. https://doi.org/10.1193/1.2218591

17 Lenz JA and Baise LG (2007). "Spatial variability of liquefaction potential in regional mapping using CPT and SPT data". *Soil Dynamics and Earthquake Engineering*, **27**(7): 690–702. https://doi.org/10.1016/j.soildyn.2006.11.005

18 Maurer BW, Green RA, Cubrinovski M and Bradley BA (2014). "Evaluation of the liquefaction potential index for assessing liquefaction hazard in Christchurch, New Zealand". *Journal of Geotechnical and Geoenvironmental Engineering*, **140**(7): (04014032)1–11. https://doi.org/10.1061/(ASCE)

GT.1943-5606.0001117

19 Rashidian V and Gillins DT (2018). "Modification of the liquefaction potential index to consider the topography in Christchurch, New Zealand". *Engineering Geology*, **232**(2018): 68–81. https://doi.org/10.1016/j.enggeo.2017.11.010

20 Maurer BW (2018). *Towards multi-tier modeling of liquefaction impacts on transportation infrastructure*. Report Project #1132-NCTRBM, Pacific Earthquake Engineering Research Centre. https://peer.berkeley.edu/sites/default/files/peer-tsrp-maurer-web20180423.pdf

21 Zhu J, Baise LG and Thompson EM (2017). "An updated geospatial liquefaction model for global application". *Bulletin of the Seismological Society of America*, **107**(3): 1365–1385. https://doi.org/10.1785/0120160198

22 Maurer B (2017). "Field-testing liquefaction models based on geospatial vs. geotechnical data". *6th International Young Geotechnical Engineers' Conference (iYGEC6) (2017, September 16-17)*, Seoul, Korea. https://digital.lib.washington.edu/researchworks/bitstream/handle/1773/39748/iYGEC6_Full\%20Paper_BWMaurer.pdf

23 Russell J and van Ballegooy S (2015). *Canterbury Earthquake Sequence: Increased Liquefaction Vulnerability Assessment Methodology*. Report Job No: 52010.140.v1.0, Tonkin & Taylor Ltd. https://d2h44nai6dnz3i.cloudfront.net/1002/2015_10_16_canterbury_earthquake_sequence_increased_liquefaction_vulnerability_assessment_methodology_tt_report_final.pdf

24 Geyin M, Baird AJ and Maurer BW (2020). "Field assessment of liquefaction prediction models based on geotechnical versus geospatial data, with lessons for each". *Earthquake Spectra*, **36**(3): 1386–1411. https://doi.org/10.1177\%2F8755293019899951

25 Rashidian V and Baise LG (2020). "Regional efficacy of a global geospatial liquefaction model". *Engineering Geology*, **272**(2020): 105644. https://doi.org/10.1016/j.enggeo.2020.105644

26 Lin A, Wotherspoon L, Bradley B and Motha J (2021). "Evaluation and modification of geospatial liquefaction models using land damage observational data from the 2010–2011 Canterbury Earthquake Sequence". *Engineering Geology*, **287**: 106099. https://doi.org/10.1016/j.enggeo.2021.106099

27 Zhu J, Daley D, Baise LG, Thompson EM, Wald DJ and Knudsen KL (2015). "A geospatial liquefaction model for rapid response and loss estimation". *Earthquake Spectra*, **31**(3): 1813–1837. https://doi.org/10.1193/121912eqs353m

28 Massey CI, Townsend DT, Lukovic B, Morgenstern R, Jones K, Rosser B and de Vilder S (2020). "Landslides triggered by the Mw7.8 14 November 2016 Kaikōura earthquake: an update". *Landslides*, **17**(10): 2401–2408. https://doi.org/10.1007/s10346-020-01439-x

29 Davies AJ, Sadashiva V, Aghababaei M, Barnhill D, Costello SB, Fanslow B, Headifen D, Hughes MW, Kotze R and Mackie J (2017). "Transport infrastructure performance and management in the South Island of New Zealand, during the first 100 days following the 2016 Mw 7.8 Kaikōura earthquake". *Bulletin of the New Zealand Society for Earthquake Engineering*, **50**(2): 271–299. https://doi.org/10.5459/bnzsee.50.2.271-299

30 Dellow S, Massey C, Cox S, Archibald G, Begg J, Bruce Z, Carey J, Davidson J, Pasqua FD, Glassey P, Hill M, Jones K, Lyndsell B, Lukovic B, McColl S, Rattenbury M, Read S, Rosser B, Singeisen C, Townsend D, Villamor P, Villeneuve M, Godt J, Jibson R, Allstadt K, Rengers F, Wartman J, Rathje E, Sitar N, Adda AZ, Manousakis J and Little M (2017). "Landslides caused by the Mw7.8 Kaikōura earthquake and the immediate response". *Bulletin of the New Zealand Society for Earthquake Engineering*, **50**(2). https://doi.org/10.5459/bnzsee.50.2.106-116

31 Kaiser A, Balfour N, Fry B, Holden C, Litchfield N, Gerstenberger M, D'Anastasio E, Horspool N, McVerry G, Ristau J, Bannister S, Christophersen A, Clark K, Power W, Rhoades D, Massey C, Hamling I, Wallace L, Mountjoy J, Kaneko Y, Benites R, Van Houtte C, Dellow S, Wotherspoon L, Elwood K and Gledhill K (2017). "The 2016 Kaikōura, New Zealand, Earthquake: Preliminary Seismological Report". *Seismological Research Letters*, **88**(3): 727–739. https://doi.org/10.1785/0220170018

32 Bastin SH, Stringer M, Green R, Wotherspoon L, van Ballegooy S, Cox BR and Osuchowski A (2018). "Geomorphological controls on the distribution of liquefaction in Blenheim, New Zealand, during the 2016 Mw7.8 Kaikoura Earthquake". *Geotechnical Earthquake Engineering and Soil Dynamics V*, pp. 264–272. https://doi.org/10.1061/9780784481455.026

33 Stringer ME, Bastin S, McGann CR, Cappellaro C, Kortbawi ME, McMahon R, Wotherspoon LM, Green RA, Aricheta J, Davis R, McGlynn L, Hargraves S, Ballegooy SV, Cubrinovski M, Bradley BA, Bellagamba X, Foster K, Lai C, Ashfield D, Baki A, Zekkos A, Lee R and Ntritsos N (2017). "Geotechnical aspects of the 2016 Kaikōura earthquake on the South Island of New Zealand". *Bulletin of the New Zealand Society for Earthquake Engineering*, **50**(2). https://doi.org/10.5459/bnzsee.50.2.117-141

34 QuakeCoRE (2009). *Historic Earthquake Events*. GIS Shapefile, https://projectorbit.maps.arcgis.com/apps/webappviewer/index.html (Accessed on 27 October 2020).

35 Cubrinovski M, Bray JD, De La Torre C, Olsen MJ, Bradley BA, Chiaro G, Stocks E and Wotherspoon L (2017). "Liquefaction effects and associated damages observed at the Wellington CentrePort from the 2016 Kaikoura earthquake". *Bulletin of the New Zealand Society for Earthquake Engineering*, **50**(2). https://doi.org/10.5459/bnzsee.50.2.152-173

36 Survey UG (2016). *M 7.8 – 54km NNE of Amberley, New Zealand, 2016-11-13 11:02:56 (UTC)*. kmz file, https://earthquake.usgs.gov/earthquakes/eventpage/us1000778i/shakemap/pgv (Accessed on 21 December 2019).

37 Hijmans RJ, Cameron SE, Parra JL, Jones PG and Jarvis A (2005). "Very high resolution interpolated climate surfaces for global land areas". *International Journal of Climatology*, **25**(15): 1965–1978. https://doi.org/10.1002/joc.1276

38 Wald DJ and Allen TI (2007). "Topographic slope as a proxy for seismic site conditions and amplification". *Bulletin of the Seismological Society of America*, **97**(5): 1379–1395. https://doi.org/10.1785/0120060267

39 Foster KM, Bradley BA, McGann CR and Wotherspoon LM (2019). "A VS30 Map for New Zealand based on geologic and terrain proxy variables and field measurements". *Earthquake Spectra*, **35**(4): 1865–1897. https://doi.org/10.1193\%2F121118EQS281M

40 Fan Y, Li H and Miguez-Macho G (2013). "Global patterns of groundwater table depth". *Science*, **339**(6122): 940–943. https://doi.org/10.1126/science.1229881

41 Westerhoff RS and White PA (2014). *Application of equilibrium water table estimates using satellite measurements to the Canterbury Region, New Zealand*. Report GNS Science

Report 2013/43 25 p, GNS Science.

42 Westerhoff R, White P and Miguez-Macho G (2018). "Application of an improved global-scale groundwater model for water table estimation across New Zealand". *Hydrology and Earth System Sciences*, **22**(12): 6449–6472. https://doi.org/10.5194/hess-22-6449-2018

43 HydroSHEDS (2006). *River Network (Stream Lines) at 30 s Resolution*. GIS Shapefile, https://www.hydrosheds.org/page/hydrorivers (Accessed on 27 August 2019).

44 Lehner B, Verdin K and Jarvis A (2006). *HydroSHEDS technical documentation*. Report, World Wildlife Fund. https://www.hydrosheds.org/images/inpages/HydroSHEDS_TechDoc_v1_2.pdf

45 Lehner B, Verdin K and Jarvis A (2008). "New global hydrography derived from spaceborne elevation data". *EOS Transactions American Geophysical Union*, **89**(10): 93–94. https://doi.org/10.1029/2008eo100001

46 Ministry of Environment (2010). *River Environment Classification New Zealand (2010)*. GIS Shapefile, https://data.mfe.govt.nz/layer/51845-river-environment-classification-new-zealand-2010/ (Accessed on 4 March 2019).

47 Land Research New Zealand (2010). *New Zealand Land Resource Information (NZLRI) Slope*. Geotiff, https://lris.scinfo.org.nz/license/landcare-data-use-licence-v1/ (Accessed on 9 November 2020).

48 Crown Minerals (2009). *NZ Land Extent and Coastline*. GIS Shapefile, http://www.crownminerals.govt.nz/cms/pdf-library/petroleum-blocks-offers-1/northland-and-raukumara-block-offers/northland-shapefiles-5-5-mb-pdf/view (Accessed on 23 August 2018).

49 NASA (2009). *Distance to the Nearest Coast*. csv file, https://oceancolor.gsfc.nasa.gov/docs/distfromcoast/ (Accessed on 3 January 2020).

50 Land Information New Zealand (2012). *NZ 8 m Digital Elevation Model*. Geotiff, https://data.linz.govt.nz/layer/51768-nz-8m-digital-elevation-model-2012/ (Accessed on 10 March 2021).

51 Cubrinovski M, Rhodes A, Ntritsos N and Van Ballegooy S (2019). "System response of liquefiable deposits". *Soil Dynamics and Earthquake Engineering*, **124**: 212–229. https://doi.org/10.1016/j.soildyn.2018.05.013